Research Article

Ran Guo, Changlong Zhang, Liwei Xue, Xuan Li*, Liguo Chen*, and Zhou Zheng*

Fabrication of PDMS nano-mold by deposition casting method

https://doi.org/10.1515/ntrev-2025-0149
received December 27, 2024; accepted February 24, 2025

Abstract: Nanoimprinting is a high-throughput, low-cost, and high-precision nanofabrication technology. In this article, we proposed a method for fabricating PDMS nano-molds by side etching deposition casting. During the fabrication process, we used a wet etching method to obtain the etching width, a nanogap was formed when the deposition process was completed, and finally, the nanochannel was obtained by the lift-off method. Then, the casting method was used to replicate the nanochannel pattern to create the polydimethylsiloxane (PDMS) nano-mold. The effect of development time on the morphology of photoresist patterns was studied, the relationship between etching time and etching width was analyzed, and the effect of different deposition methods on the formation of nanochannels was studied. We believe that the proposed method can play a certain role in promoting the development of nanotechnology and nanoscience.

1 Introduction

The level of nanomanufacturing technology has become an important indicator to measure a country's manufacturing capabilities and represents the forefront of the development of manufacturing science. Nanofabrication technology is an important means to manufacture nanostructures and devices. Nanostructures and devices have excellent physical properties and unique structural characteristics and are widely used in micro-nano optics [1–3], micro-nano fluids [4–6], and biomedicine [7–9]. Therefore, nanofabrication technology is very important to meet the urgent needs of various applications.

So far, there are many nano-manufacturing technologies. A focused ion beam uses high energy to bombard samples to remove surface materials and can directly carve micro-nano channels without masks and additional etching processes to achieve direct writing effects [10–12]. However, due to its serial and time-consuming manufacturing characteristics, it is not an efficient and economical manufacturing method [13–15]. Interference lithography is a maskless lithography method that uses light and dark light field distribution to produce periodic micro-nano structure patterns over a large area without expensive equipment and with a short process cycle [16–18]. However, this technology can only produce limited patterns, so its application is limited to micro-nano devices with simple periodic channels [19,20]. The crack method is a new high-throughput micro-nano manufacturing technology that uses stress concentration to create an array of micro-nano cracks. It has a simple process, high efficiency, and low cost [21–23]. However, the crack position and number are difficult to control [24–26]. In addition, the uneven tensile stress intensity can easily lead to uneven crack size.

In contrast, nanoimprint lithography is a high-precision, high-throughput, low-cost nanomanufacturing technology that can produce patterns below 10 nm [27–29]. However, the quality of nanoimprinted patterns is mainly limited by the quality of the nano-mold [30–33]. Rao *et al.* proposed a method for preparing convex silicon nano-molds based on sidewall technology and finally obtained convex silicon nano-molds with a scale of less than 200 nm [34]. Yin *et al.* proposed a method for manufacturing concave silicon nano-molds based on tilted evaporation technology. They combined ultraviolet lithography, tilted evaporation, and sputtering etching processes to prepare large-scale concave silicon nano-molds with a scale of less than 100 nm [35]. Sun *et al.* proposed a method for manufacturing convex silicon nano-molds based on proximity ultraviolet lithography technology. The required size of the photoresist pattern is

* **Corresponding author: Xuan Li**, School of Mechanical and Electrical Engineering, Soochow University, Suzhou, Jiangsu, 215137, China, e-mail: xuanli@suda.edu.cn
* **Corresponding author: Liguo Chen,** School of Mechanical and Electrical Engineering, Soochow University, Suzhou, Jiangsu, 215137, China, e-mail: chenliguo@suda.edu.cn
* **Corresponding author: Zhou Zheng**, School of Mechanical and Electrical Engineering, Soochow University, Suzhou, Jiangsu, 215137, China, e-mail: zzheng2023@suda.edu.cn
Ran Guo, **Changlong Zhang**, **Liwei Xue:** School of Mechanical and Electrical Engineering, Soochow University, Suzhou, Jiangsu, 215137, China

obtained by controlling the exposure gap between the mask and the photoresist. Finally, a convex silicon nano-mold with a size of 263 nm is obtained using deep reactive ion etching technology with the photoresist as a mask [36]. However, all the aforementioned processes require expensive dry etching equipment, and silicon nano-molds have high brittleness. During the nanoimprint process, they are prone to brittle cracking due to uneven stress or temperature changes.

To address the aforementioned problems, this article proposes a method for manufacturing convex polydimethylsiloxane (PDMS) nano-molds by side etch deposition casting. By optimizing the wet etching parameters, different etching widths were obtained. After wet etching, the nanochannel was obtained by combining deposition technology and lift-off process. The nanochannel pattern was replicated by the PDMS casting method to obtain a convex PDMS nano-mold with a size of less than 100 nm. In the process of manufacturing convex PDMS nano-molds, the effect of development time on photoresist patterns was studied, the influence of wet etching time on nanochannel size was revealed, and the impact of different metal deposition processes on the formation of nanochannels was analyzed. PDMS nano-molds have characteristics such as good flatness, low cost, and easy demolding, can be used repeatedly, and have a long life. It provides a new method for low-cost and high-precision preparation of nano-molds.

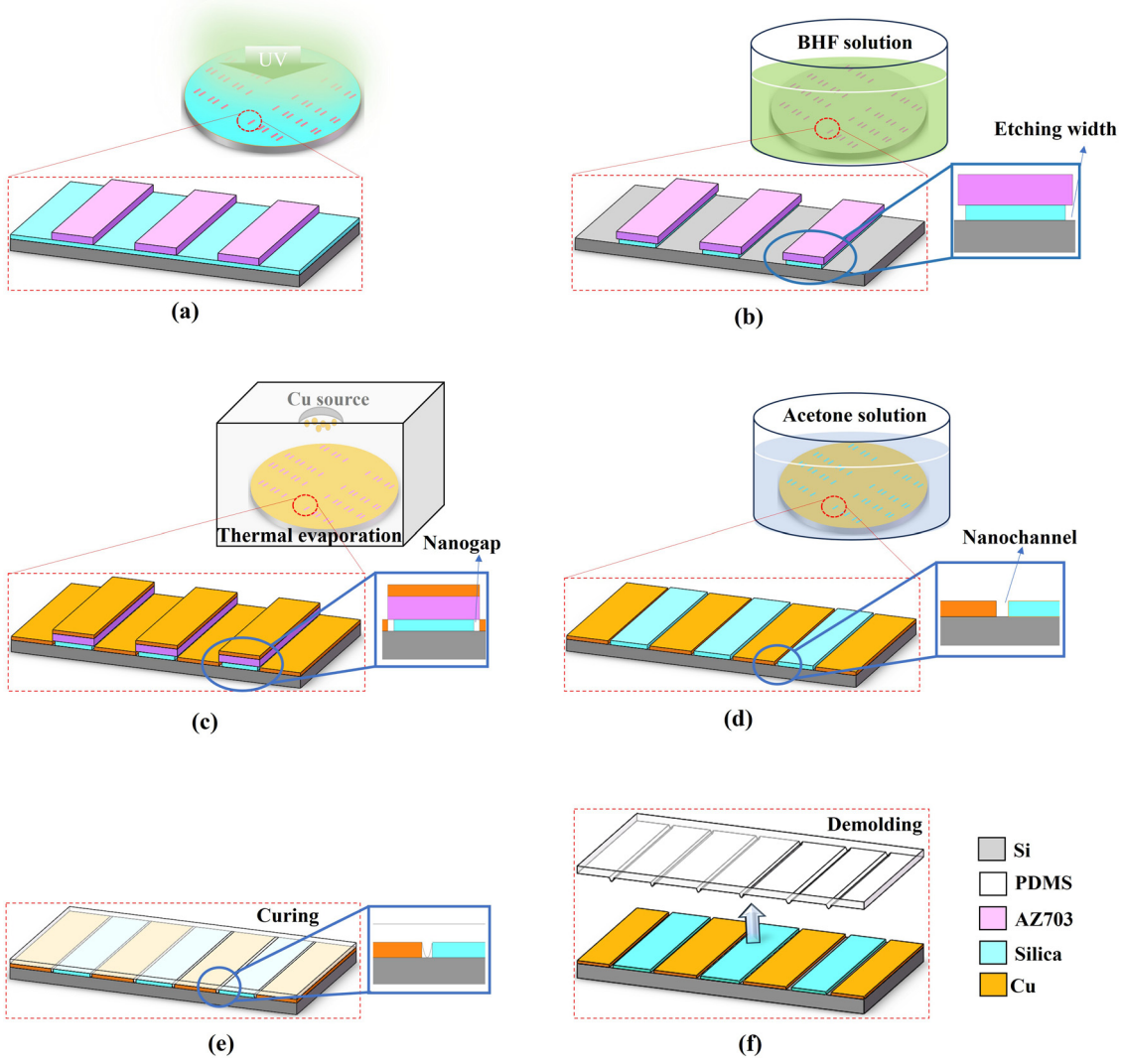

Figure 1: Illustration of PDMS nano-mold fabrication process. (a) UV photolithography, (b) wet etching, (c) Cu deposition, (d) lift-off, (e) PDMS casting, and (f) demolding.

2 Experiments

The PDMS nano-mold can be fabricated in six steps: ultraviolet (UV) photolithography, wet etching, Cu deposition, Lift-off, PDMS casting, and demolding, as shown in Figure 1.

In Figure 1(a) showing UV photolithography, a silicon wafer with a ~100 nm silica thickness was selected as the substrate. The AZ703 photoresist was spin coated on the silica at a speed of 4,000 rpm for 30 s and prebaked at 85°C for 30 min. With a mask containing a 5 μm wide and 4 mm long line grating photomask, the photoresist was exposed to UV light for 30 s by a mask aligner (MA/BA6, SUSS MicroTec, Germany). After developing in developer for 60 s, micro photoresist mesas were obtained.

In Figure 1(b) showing wet etching, after the photoresist was developed, the sample was then wet etched with buffered hydrofluoric acid (BHF) solution ($HF:NH_4F$:water = 3:6:10, v:v:v) in a 60°C water bath, then washed in deionized water, and dried under the nitrogen flow.

In Figure 1(c) showing Cu deposition, before Cu deposition, the sample was treated with oxygen plasma treatment for 1 min to remove any residues and enhance the bonding of the Cu metal film to the deposition substrate. The Cu deposition was carried out in a thin film deposition system (Kurt J. Lesker LAB18, Pittsburgh, US). The chamber pressure was maintained at 2.3–2.33 mTorr, and the radio frequency powder was 150 W. The nanogap can therefore be fabricated. Cu was selected as the deposition material in this process due to its inexpensiveness, further reducing the fabrication cost.

In Figure 1(d) showing lift-off, the sample after thermal evaporation was placed in an acetone solution and soaked for 30 min, and then the photoresist was gently lifted off with a cotton ball to obtain a nanochannel.

In Figure 1(e) showing PDMS casting, the sample with nanochannels was placed in a trimethylchlorosilane atmosphere for hydrophobic treatment for 20 min. Then, a 5:1 mixed solution of PDMS and curing agent was cast on the hydrophobic nanochannels, placed in a 10 Pa vacuum environment for 1 h, and then placed in a 60°C oven for curing for 4 h.

In Figure 1(f) showing demolding, after cooling to room temperature, the sample poured with the PDMS mixed solution was taken out of the oven, and the cured PDMS was gently separated from the sample to obtain a convex PDMS nano-mold.

3 Results and discussion

3.1 The influence of development time on the morphology of photoresist mesas

The soluble area of photoresist caused by exposure dissolved in the chemical developer is called photoresist development. Its main purpose is to copy the mask pattern into the photoresist accurately. If the development process is not controlled correctly, the photoresist pattern will have problems. The three main development problems are underdevelopment, incomplete development, and overdevelopment. Figure 2 shows three types of problematic developed photoresists compared to correctly developed photoresists. Underdeveloped photoresist patterns are wider and have a certain slope compared to normal (Figure 2(a) and (e)). The incomplete development of

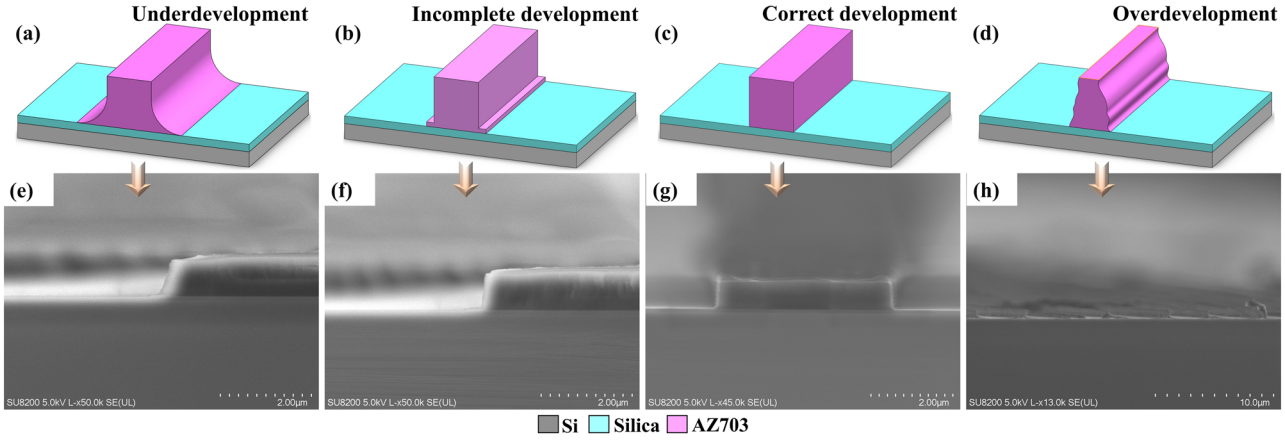

Figure 2: Photoresist development issues. (a) and (e) Schematic diagram and SEM image of photoresist underdevelopment, (b) and (f) schematic diagram and SEM image of incomplete photoresist development, (c) and (g) schematic diagram and SEM image of correct photoresist development, and (d) and (h) schematic diagram and SEM image of photoresist overdevelopment.

photoresist patterns will leave a thin photoresist layer on the substrate (Figure 2(b) and (f)). Overdevelopment is due to the prolonged development time, which removes too much photoresist, causing the photoresist pattern to narrow and be damaged (Figure 2(d) and (h)).

It can be seen that the development time directly affects the morphology of the photoresist pattern, thereby affecting the subsequent processing technology. Therefore, it is necessary to study the effect of development time on the morphology of the photoresist pattern. Figure 3 shows the microscopic images and scanning electron microscopy (SEM) image at different development times. When the development time is 30 s, the pattern lines of the photoresist are clear (Figure 3(a)), and the sidewalls of the photoresist are steep (Figure 3(b)), which is the optimal development time. When the development time is extended to 45 s, local corrosion occurs in the photoresist pattern, and a large number of corrosion points can be seen in the microscope image (Figure 3(c)). When the development time is 90 s, the photoresist pattern collapses and distorts. If the time is further extended, the photoresist pattern may even disappear.

3.2 The influence of etching time on etching width

Etching time seriously affects the etching width and thus the nanochannel size. Therefore, it is necessary to study the effect of etching time on etching width. Figure 4 shows the cross-sectional profiles of the etched sample, the SEM (SU8220, Hitachi, Japan) images are shown on the left (Figure 4(a)), and the schematic diagram listing the dimensions of the etched sample is shown on the right (Figure 4(b)).

Because wet etching has the inherent property of etching any exposed surface, that is, isotropic etching. Therefore, during the initial stages of wet etching, the sidewalls are usually etched at a rate similar to the bottom, producing a lateral undercut distance of the same order as the etching depth, resulting in a curve profile whose radius is approximately equal to the etching depth, as shown in Figure 5(a), where the size of W_0 is approximately equal to H. When the etching time exceeds 11 s, the front of the etchant meets the stop layer (Si layer), the consumption of the etchant becomes less, the etching begins to accelerate in the horizontal direction, and the etching width gradually

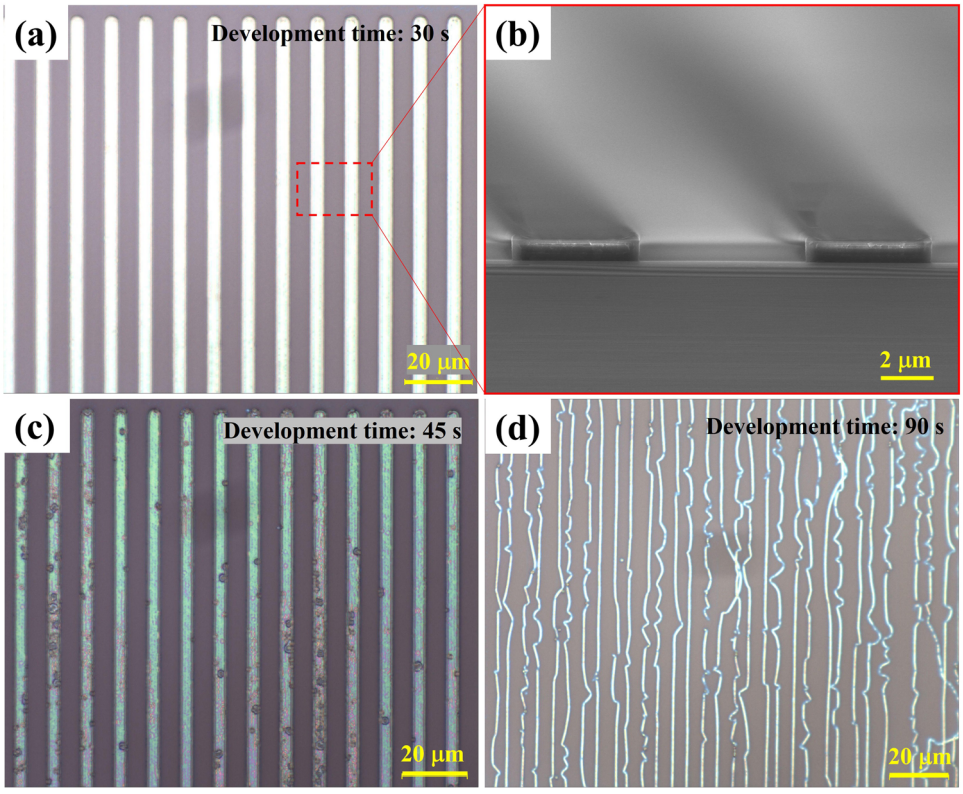

Figure 3: Microscopic images of photoresists under different development times. (a) 30 s, (b) SEM image of photoresist with development time of 30 s, (c) 45 s, and (d) 90 s.

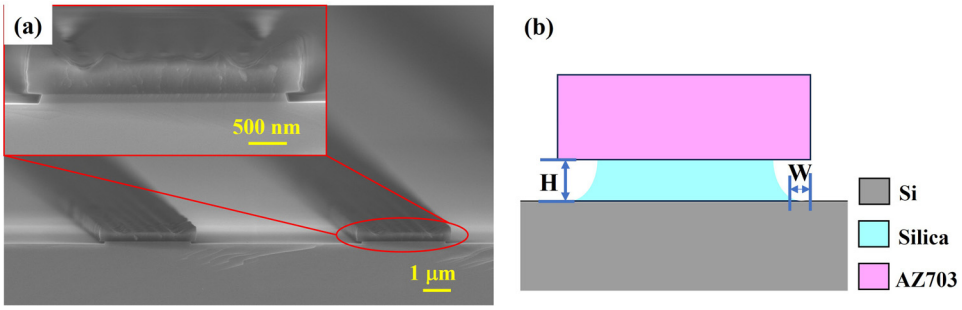

Figure 4: Schematic diagram of the wet etching process. (a) SEM image of the etched sample, (b) schematic diagram listing the dimensions of the etched sample (*W* is the etching width (*t* > 11 s), and *H* is the depth of nanochannel equal to the etching thickness of silica).

increases, and the SiO_2 sidewalls gradually straighten, as shown in Figure 5(d).

From the curve of the relationship between etching time and etching width (Figure 6), it can be seen that as the etching time increases, the etching width gradually increases. The etching width could be predicted from the etching time by the following formula:

$$W = 1.31t^{1.62} \quad (t > 11), \tag{1}$$

where t is the etching time and W is the etching width. The average correlation of curve fitting can reach $R^2 = 0.97$, indicating good agreement between experimental data and fitting data.

3.3 The reproducibility of the wet etching process

To study the reproducibility of the wet etching process, the samples were placed in the BHF solution and three different samples were wet etched with silica in a 60°C water bath for 15 s (Figure 7). The etching width of the three samples was measured. Their dimensions were as follows: (a) etching width was 108 ± 3 nm, (b) etching width was 106 ± 3 nm, and (c) etching width was 110 ± 1 nm. The maximum width difference in etching width between chips is 4 nm, the average etching width is 114 nm, and the width variation is about 4%. It can be seen that the BHF wet etching process has good repeatability.

3.4 The influence of metal deposition methods on the formation of nanogap

Figure 8 shows the schematic and SEM images of nanogap obtained at different angles of thermal evaporation.

Magnetron sputtering deposition has isotropic characteristics (Figure 8(a)) and has the advantages of good

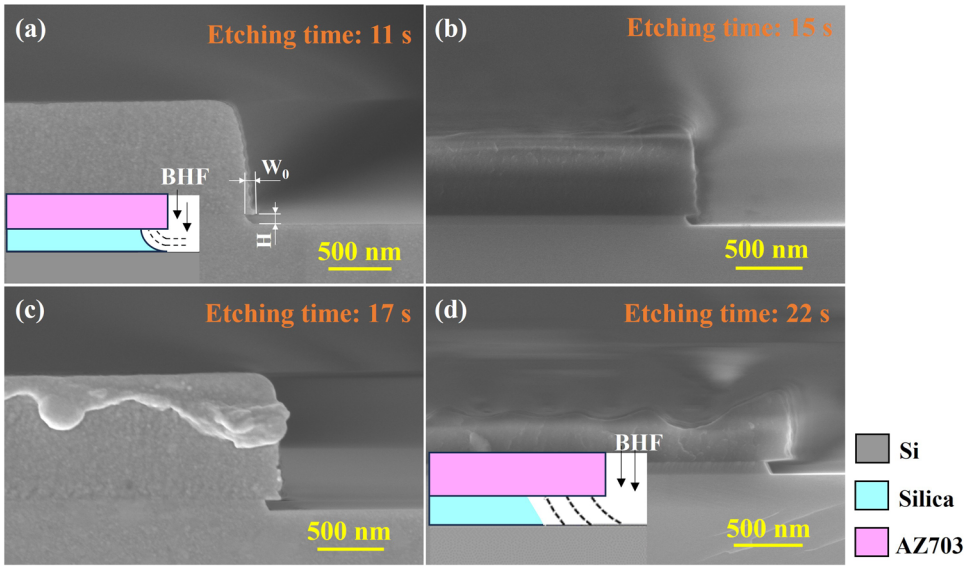

Figure 5: The SEM images of the etched sample under different etching times. (a) etching time 11 s, (b) etching time 15 s, (c) etching time 17 s, and (d) etching time 22 s.

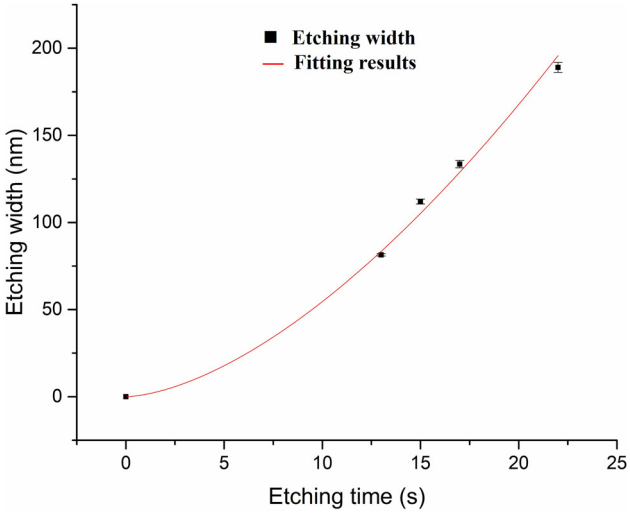

Figure 6: Relationship between etching time and etching width.

deposition quality, uniform film thickness, and good bonding strength between the film and the substrate. Using magnetron sputtering deposition, the metal film will be evenly deposited on the target substrate, such as the horizontal surface of the photoresist, the side wall of the photoresist, the silicon substrate, and the junction between the photoresist and the substrate (Figure 8(c)). Therefore, in the subsequent lift-off process, the metal film is easy to tear and is not easy to form nanochannels (Figure 8(e)).

Unlike magnetron sputtering deposition, thermal evaporation has anisotropic characteristics (Figure 8(b)) and has the advantages of a simple process, short deposition time, and good deposition directionality. During the thermal evaporation process, the metal film on the side wall of the photoresist is not connected to the metal film on the silicon substrate (Figure 8(d)). After the sample was lifted off, there was no connection between the metal film on the photoresist and the metal film on the substrate, indicating that thermal evaporation cannot form sealed nanotubes. After being lifted off, the metal film on the photoresist is not connected to the metal film on the substrate, so no tearing occurs, thus forming a nanochannel (Figure 8(f)). Therefore, thermal evaporation is more suitable for this process.

3.5 Fabrication of polymer nanochannel using the PDMS nano-mold

Figure 9 shows SEM images of nanochannels at different etching times. As the figure shows, the nanochannel size can be effectively controlled by changing the etching time. As the etching time increases, the nanochannel width gradually increases. When the etching time was 13 s, a nanochannel with a size of 82 nm in width and 56 nm in depth was obtained (Figure 9(a)). However, nanochannels based on silicon substrates are prone to brittle cracks if they are directly used as molds for hot embossing. Therefore, this article pours PDMS on the nanochannels to replicate the nanochannel pattern, thereby obtaining a convex PDMS nano-mold, in which the nano-ridge width is 82 ± 7 nm and the height is 40 ± 6 nm (Figure 10(a) and (b)). PDMS has good flatness and is easy to de-mold [37,38]. The SU-8

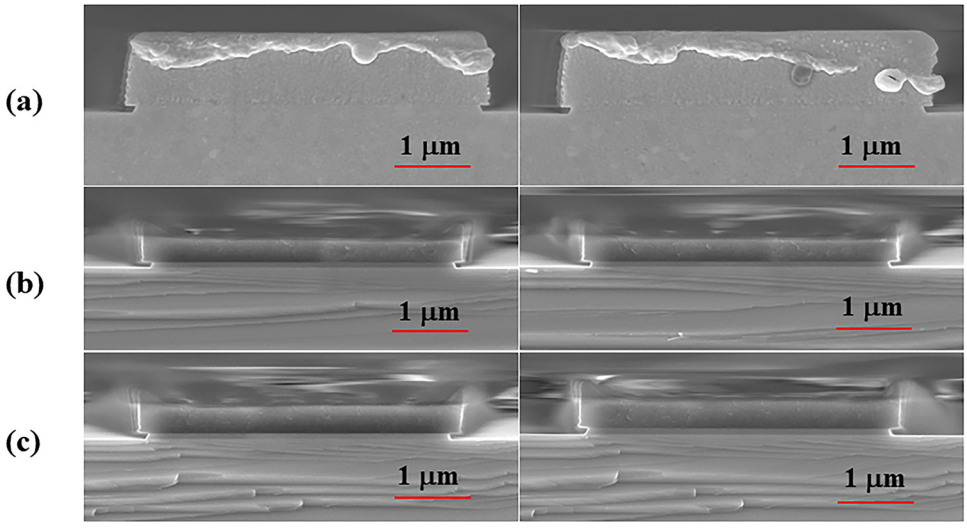

Figure 7: SEM images of etching width etched by BHF in different chips. The SEM images of (a)–(c) show the etching width from three samples. The etching time is 15 s: (a) 108 ± 3 nm, (b) 106 ± 3 nm, and (c) 110 ± 1 nm.

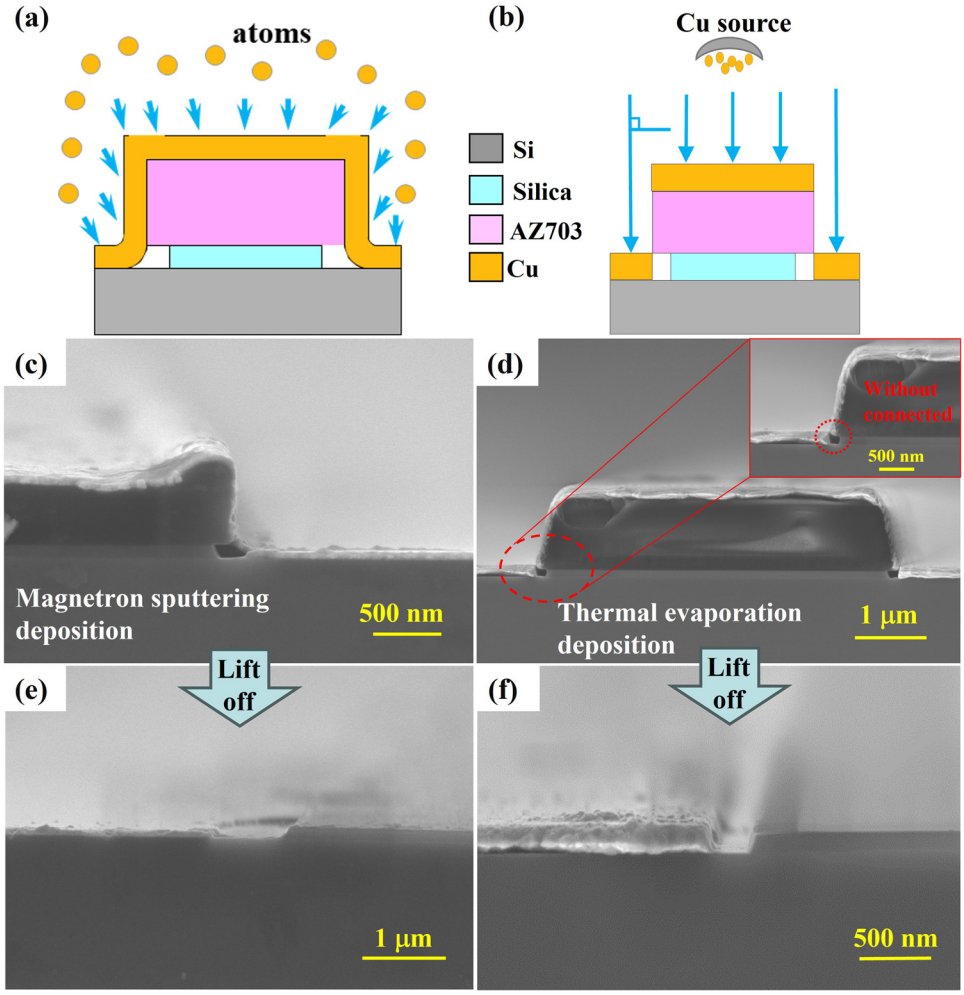

Figure 8: Schematic and SEM images of nanogap and nanochannel obtained under different metal deposition methods. (a) schematic diagram of magnetron sputtering deposition, (b) schematic diagram of thermal evaporation deposition, (c) SEM image of nanotube obtained by magnetron sputtering deposition, (d) SEM image and enlarged image of nanotubes obtained by thermal evaporation deposition, (e) SEM image of nanochannel obtained after lift-off using magnetron sputtering deposition method, and (f) SEM image of nanochannel obtained after lift-off using thermal evaporation deposition method.

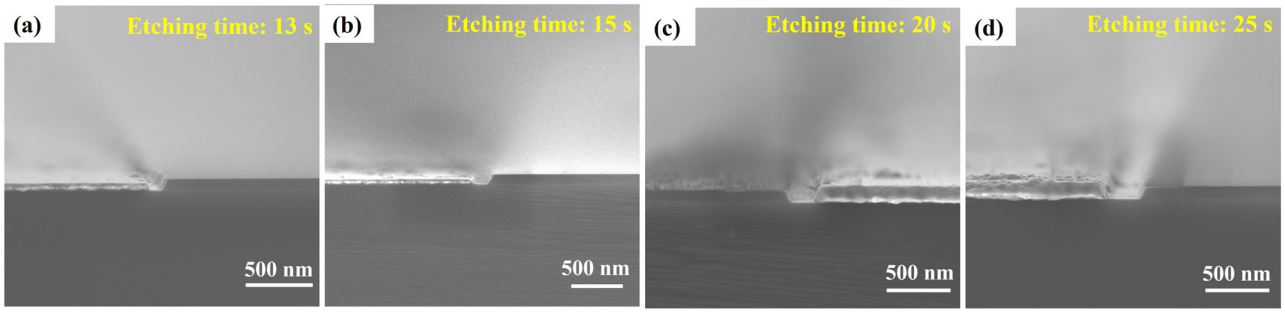

Figure 9: SEM images of nanochannel obtained under different etching times. (a) 82 nm wide and 56 nm deep nanochannel resulting from etching time of 13 s, (b) 108 nm wide and 55 nm deep nanochannel resulting from etching time of 15 s, (c) 167 nm wide and 86 nm deep nanochannel resulting from etching time of 20 s, and (d) 242 nm wide and 88 nm deep nanochannel resulting from etching time of 25 s.

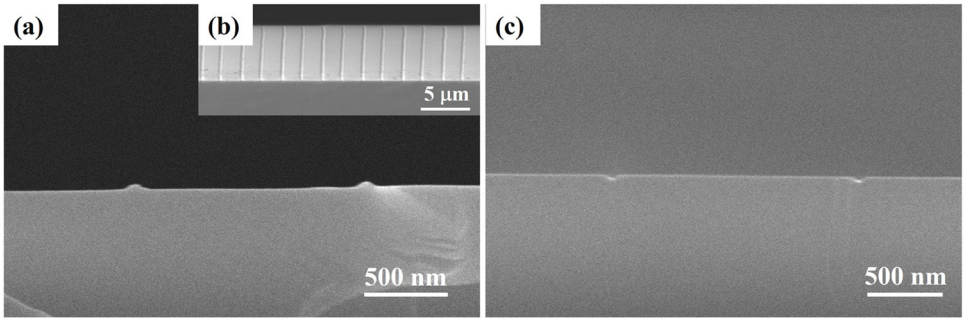

Figure 10: SEM images of PDMS nano-mold and SU-8 nanochannel: (a) PDMS nano-mold with a width of 82 ± 7 nm and a height of 40 ± 6 nm, (b) SEM image of PDMS nano-mold, and (c) SU-8 nanochannel width 74 ± 9 nm, depth 37 ± 7 nm.

photoresist was imprinted with a convex PDMS nano-mold at 85°C for 20 min to transfer the nanopattern to the SU-8 substrate, and finally, a nanochannel with a width of 74 ± 9 nm and a depth of 37 ± 7 nm was obtained.

PDMS nano-molds with sizes less than 100 nm were successfully prepared by the deposition casting method proposed in this study. With this method, different sizes of nanochannels can be obtained by precisely controlling the wet etching parameters. In future studies, the duty cycle of the nanochannels can also be adjusted by changing the width of the photoresist mesas. However, there are still some limitations of this method that need to be overcome: (1) Since wet etching has the characteristic of isotropic etching, the preparation of molds by this method cannot produce molds with a width less than the depth. In future research, only the silica layer and the metal layer can be used as a mask, and then the dry etching process is used to etch the silicon substrate, and the silicon nano-molds with a higher depth-to-width ratio can be obtained by optimizing the parameters of the dry etching, but its production cost will also be greatly increased. Alternatively, metal deposition or parylene film deposition is performed on the mold after the lift-off process. Since the thickness of the metal and silica layer deposited on the surface by the deposition technique is much thicker compared to the thickness deposited on the sidewalls of the nanochannel and on the bottom of the nanochannel, the depth of the nanochannel increases rapidly, resulting in molds with widths that are less than the depth. (2) The nano-ridges on the PDMS nano-mold are not perfectly straight. A slight unevenness in the lines of the photolithography mask used in this study caused deformation, which led to a series of deformations in the silica layer, photoresist, and nanochannels. It is highly recommended that a photolithography mask with higher accuracy be used in future studies.

4 Conclusions

In this study, a sub-100 nm PDMS nano-mold was successfully fabricated by the side etching deposition casting method. We studied the effect of development time on the morphology of photoresists. A slope or a layer of stepped film at the bottom of the photoresist results from the development time being too short, which prevents the development solution from completely reacting with the photoresist. Overly extended development times can cause the photoresist to disintegrate or vanish. The influence of etching time on etching width was investigated. The impact of thermal evaporation and magnetron sputtering deposition methods on the formation of nanochannels was analyzed, and it was found that the anisotropic deposition characteristics of thermal evaporation better meet the needs of nanochannel preparation technology. Finally, PDMS nano-mold with a width of 82 ± 7 nm and a height of 40 ± 6 nm was prepared under optimized parameters.

Acknowledgments: The authors are grateful for the reviewers valuable comments that improved the manuscript.

Funding information: This research work was supported by the Excellent Postdoctoral Program of Jiangsu Province (No. 2023ZB694).

Author contributions: All authors have accepted responsibility for the entire content of this manuscript and approved its submission.

Conflict of interest: The authors state no conflict of interest.

Data availability statement: The datasets generated and/or analyzed during the current study are available from the corresponding author on reasonable request.

References

[1] Kasani S, Curtin K, Wu N. A review of 2D and 3D plasmonic nanostructure array patterns: fabrication, light management and sensing applications. Nanophotonics. 2019;8(12):2065–89.

[2] Zhao ZJ, Ahn J, Hwang SH, Ko J, Jeong Y, Bok M, et al. Large-area nanogap-controlled 3D nanoarchitectures fabricated via layer-by-layer nanoimprint. ACS Nano. 2021;15(1):503–14.

[3] Jia Y, Chen F. Recent progress on femtosecond laser micro-/nano-fabrication of functional photonic structures in dielectric crystals: A brief review and perspective. APL Photonics. 2023;8(9):090901.

[4] Zhang X, Liu H, Jiang L. Wettability and applications of nanochannels. Adv Mater. 2019;31(5):e1804508.

[5] Feng HQ, Shen ST, Jin ML, Zhang QL, Liu MJ, Wu ZH, et al. Microwell confined electro-coalescence for rapid formation of high-throughput droplet array. Small. 2023;19(45):2302998.

[6] Rahman M, Islam KR, Islam MR, Islam MJ, Kaysir MR, Akter M, et al. A critical review on the sensing, control, and manipulation of single molecules on optofluidic devices. Micromachines. 2022;13(6):968.

[7] Higgins SG, Becce M, Belessiotis-Richards A, Seong H, Sero JE, Stevens MM. High-aspect-ratio nanostructured surfaces as biological metamaterials. Adv Mater. 2020;32(9):e1903862.

[8] Huang L, Yang DY, Yu ZM, He JX, Chen Y, Zhou JH. Deep learning-aided high-throughput screening of time-resolved protein crystallization on programmable microliter-droplet systems. Chem Eng J. 2022;450:138267.

[9] Alfaro JA, Bohländer P, Dai MJ, Filius M, Howard CJ, van Kooten XF, et al. The emerging landscape of single-molecule protein sequencing technologies. Nat Methods. 2021;18(6):604–17.

[10] Mahajan S, Sharkins JA, Hunter AH, Avishai A, Ereifej ES. Focused ion beam lithography to etch nano-architectures into microelectrodes. J Visualized Exp. 2020;155:e60004.

[11] Manoccio M, Esposito M, Passaseo A, Cuscuna M, Tasco V. Focused ion beam processing for 3D chiral photonics nanostructures. Micromachines. 2021;12(1):6.

[12] He S, Tian R, Wu W, Li W-D, Wang D. Helium-ion-beam nanofabrication: extreme processes and applications. Int J Extreme Manuf. 2021;3(1):012001.

[13] Li P, Chen S, Dai H, Yang Z, Chen Z, Wang Y, et al. Recent advances in focused ion beam nanofabrication for nanostructures and devices: fundamentals and applications. Nanoscale. 2021;13(3):1529–65.

[14] Tavares L, Chiriaev S, Adashkevich V, Taboryski R, Rubahn HG. Height patterning of nanostructured surfaces with a focused helium ion beam: a precise and gentle non-sputtering method. Nanotechnology. 2020;31(14):145303.

[15] Petrov YV, Grigoryev EA, Baraban AP. Helium focused ion beam irradiation with subsequent chemical etching for the fabrication of nanostructures. Nanotechnology. 2020;31(21):215301.

[16] Jee H, Park M-J, Jeon K, Jeong C, Lee J. Combining interference lithography and two-photon lithography for fabricating large-area photonic crystal structures with controlled defects. Appl Sciences-Basel. 2021;11(14):6559.

[17] Valsecchi C, Gomez Armas LE, de Menezes JW. Large area nanohole arrays for sensing fabricated by interference lithography. Sensors. 2019;19(9):2182.

[18] Hreshchuk OM, Yukhymchuk VO, Dzhagan VM, Danko VA, Minko VI, Indutnyi IZ, et al. Efficient SERS substrates based on laterally ordered gold nanostructures made using interference lithography. Semicond Phys Quantum Electron Optoelectron. 2019;22(2):215–23.

[19] Holmes J, Zhang M, Greibe T, Schaich WL, Jacobson SC, Dragnea B. Mapping complex profiles of light intensity with interferometric lithography. Nanoscale Adv. 2023;5(7):2045–53.

[20] Sasidharan V, Neumann A, Brueck SRJ. Diffraction-grating beam splitter, interferometric-lithography nanopatterning with a multi-longitudinal-mode diode laser. J Vac Sci Technol B. 2021;39(6):062603.

[21] Chen M, Wang Z, Ge X, Wang Z, Fujisawa K, Xia J, et al. Controlled fragmentation of single-atom-thick polycrystalline graphene. *Matter* . 2019;2(3):666–79.

[22] Zhang C, Wu M, Li M, Che L, Tan Z, Guo D, et al. A nanonewton-scale biomimetic mechanosensor. Microsyst Nanoeng. 2023;9:87.

[23] Zhang C, Wu M, Cao S, Liu M, Guo D, Kang Z, et al. Bioinspired environment-adaptable and ultrasensitive multifunctional electronic skin for human healthcare and robotic sensations. Small. 2023;19(41):e2304004.

[24] Namdari N, Mohammadian B, Jafari P, Mohammadi R, Sojoudi H, Ghasemi H, et al. Advanced functional surfaces through controlled damage and instabilities. Mater Horiz. 2020;7(2):366–96.

[25] Zhou Y, Zhan P, Ren M, Zheng G, Dai K, Mi L, et al. Significant stretchability enhancement of a crack-based strain sensor combined with high sensitivity and superior durability for motion monitoring. ACS Appl Mater Interfaces. 2019;11(7):7405–14.

[26] Zhang S, Liu H, Yang S, Shi X, Zhang D, Shan C, et al. Ultrasensitive and highly compressible piezoresistive sensor based on polyurethane sponge coated with a cracked cellulose nanofibril/silver nanowire layer. ACS Appl Mater Interfaces. 2019;11(11):10922–32.

[27] Chou SY. Sub-10 nm imprint lithography and applications. J Vac Sci Technol B: Microelectron Nanometer Struct. 1997;15(6):032002.

[28] Zhang L, Yan JW. Study on nano-graphitic carbon coating on Si mold insert for precision glass molding. Surf Coat Technol. 2022;448:128893.

[29] Moon J, Kwon S, Alahbakhshi M, Lee Y, Cho K, Zakhidov A, et al. Surface energy-driven preferential grain growth of metal halide perovskites: effects of nanoimprint lithography beyond direct patterning. ACS Appl Mater Interfaces. 2021;13(4):5368–78.

[30] Cates N, Einck V, Micklow L, Morere J, Okoroanyanwu U, Watkins JJ, et al. Roll-to-roll nanoimprint lithography using a seamless cylindrical mold nanopatterned with a high-speed mastering process. Nanotechnology. 2021;32(15):155301.

[31] Mizoshita N, Yamada Y, Murase M, Goto Y, Inagaki S. Direct nanoimprinting of nanoporous organosilica films consisting of covalently crosslinked photofunctional frameworks. Nanoscale. 2020;12(41):21146–54.

[32] Guo R, Yan G, Niu W, Li X. Fabrication of SU-8 polymer micro/nanoscale nozzle by hot embossing method. Nanotechnology. 2024;35(25):255301.

[33] Guo R, Li X, Niu W, Feng J. Oxygen plasma assisted room temperature bonding for manufacturing SU-8 polymer micro/nanoscale nozzle. Nanotechnol Rev. 2023;12(1):20230113.

[34] Rao J, Zou H, Syms RRA, Cheng E, Liu C. Fabrication of 2D silicon nano-mold based on sidewall transfer. Micro Nano Lett. 2011;6(1):29–33.

[35] Yin Z, Qi L, Zou H, Sun L. A novel 2D silicon nano-mold fabrication technique for linear nanochannels over a 4 inch diameter substrate. Sci Rep. 2016;6:18921.
[36] Sun L, Zou H, Sang S. A low-cost and high-efficiency method for four-inch silicon nano-mold by proximity UV exposure. Nanotechnology. 2021;33(7):075303.
[37] Zhu X, Li Y, Shi Y, Hou L, Wang G, He Z, et al. Structure–mechanical property relationships of 3D-printed porous polydimethylsiloxane films. Nanotechnol Rev. 2023;12(1):20230188.
[38] He Z, Su J, Zhu X, Li Y, Yang L, Zhang X, et al. Integrated structure-function design of 3D-printed porous polydimethylsiloxane for superhydrophobic engineering. Rev Adv Mater Sci. 2024;63(1):20240074.